Water Science & Technology

IWA PUBLISHING

Water Science & Technology Vol 84 No 2, 431 doi: 10.2166/wst.2021.231

Electrochemical degradation of DCF by boron-doped diamond anode: degradation mechanism, pathways and influencing factors

Huimin Qiu[a,b,c,*], Pingping Fan[a,b,c], Xueying Li[a,b,c] and Guangli Hou[a,b,c]

[a] Institute of Oceanographic Instrumentation, Qilu University of Technology (Shandong Academy of Sciences), Qingdao 266061, China
[b] Shandong Provincial Key Laboratory of Marine Monitoring Instrument and Equipment Technology, Qingdao 266061, China
[c] School of Ocean Technology Sciences, Qilu University of Technology (Shandong Academy of Sciences), Qingdao 266061, China
*Corresponding author. E-mail: qiuhm@qlu.edu.cn

ABSTRACT

Nonsteroidal anti-inflammatory drugs (NSAIDs) have been widely detected in wastewater and surface water, indicating that the removal of NSAIDs by wastewater treatment plants was not efficient. Electrochemical advanced oxidation technology is considered to be an effective process. This study presents an investigation of the kinetics, mechanism, and influencing factors of diclofenac (DCF) degradation by an electrochemical process with boron-doped diamond anodes. Relative operating parameters and water quality parameters are examined. It appears that the degradation follows the pseudo-first-order degradation kinetics. DCF degradation was accelerated with the increase of pH from 6 to 10. The degradation was promoted by the addition of electrolyte concentrations and current density. Humic acid and bicarbonate significantly inhibited the degradation, whereas chloride accelerated it. According to the quenching tests, hydroxyl radicals (•OH) and sulfate radicals contributed 76.5% and 6.5%, respectively, to the degradation. Sodium sulfate remains a more effective electrolyte, compared to sodium nitrate and sodium phosphate, suggesting the quenching effect of nitrate and phosphate on •OH. Major DCF transformation products were identified. According to the degradation products detected by liquid chromatography–mass spectrometry, hydroxylation and decarboxylation are the main pathways of DCF degradation; while dechlorination, chlorination, and nitro substitution are also included in this electrochemical degradation process.

Key words: boron-doped diamond (BDD), DCF, degradation pathways, electrochemical oxidation, water quality parameters

HIGHLIGHTS

- The electrochemical degradation of DCF at BDD anodes follows pseudo-first-order kinetics.
- •OH contributes more than $SO_4^{\bullet-}$, but the effect of $SO_4^{\bullet-}$ cannot be ignored.
- The presence of Cl^- significantly accelerated the degradation of DCF.
- Hydroxylation and decarboxylation are main pathways in DCF degradation.

GRAPHICAL ABSTRACT

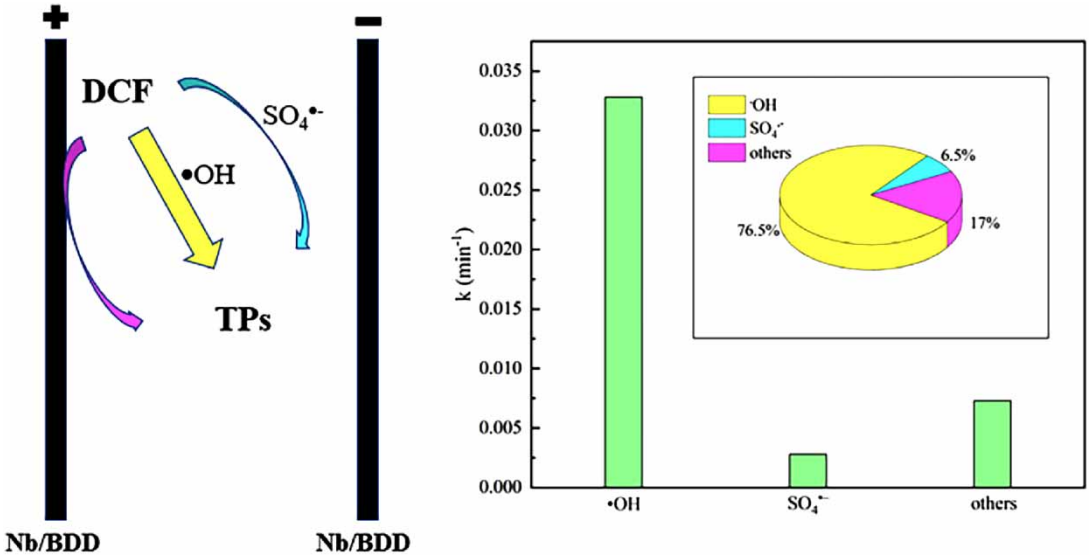

INTRODUCTION

Diclofenac (2-[(2,6-dichlorophenyl) amino] phenyl acetic acid, DCF), is one of most common nonsteroidal anti-inflammatory drugs (NSAIDs) effective in relieving pain and inflammation, and is widely used all over the world, with a yearly consumption of approximately 940 tons (Zhang *et al.* 2008). As an organic weak acid with relatively strong polarity, DCF is not likely to hydrolyze or volatilize, and it has been detected in surface water, groundwater, and wastewater concentrations ranging from ng/L to μg/L (Stuer-Lauridsen *et al.* 2000; Tauxe-Wuersch *et al.* 2005; Zorita *et al.* 2009). Such an invasive presence indicates that it cannot be effectively removed from wastewater treatment plants (WWTPs) (Lindqvist *et al.* 2005; Wu *et al.* 2019). Lishman *et al.* (2006) found 12 out of 26 samples where DCF concentrations were higher in WWTP effluent compared to influent in Ontario. Kreuzinger *et al.* (2004) reported that at least 8 days of sludge retention time were needed to significantly biodegrade DCF. The average removal rate of DCF was very low (26%) based on the sewage treatment process reported by Lindqvist *et al.* (2005). Some researchers focus on its potential toxicity to the environment (Fent *et al.* 2006; Aslan *et al.* 2020; Duarte *et al.* 2020). Oaks *et al.* (2004) referred to DCF residues as the cause of vulture population decline in Pakistan. Its testicular and epididymal toxicity also attracts attention (Owumi *et al.* 2020). Fu *et al.* (2020) found DCF residue in water to be biotransformed by *Gammarus pulex* and *Hyalella azteca*, representing a 25 to 110-fold increase of bioconcentration factors. The safe and effective removal of DCF residue has been a growing concern. Adsorption and advanced oxidation process such as photodegaradation are commonly known methods for the removal of pharmaceutical drugs (Ali *et al.* 2016; Sharma *et al.* 2018; Balasubramani *et al.* 2020; Dhiman *et al.* 2021). Ultrasonic, ozonation, the Fenton process, photocatalysis, chlorine oxidation, and electrolysis have been studied to examine and compare the removal effect on DCF (Huber *et al.* 2003; Brillas *et al.* 2010; Nie *et al.* 2014; Wang *et al.* 2014; Wang *et al.* 2015a; Kumar *et al.* 2020; Li *et al.* 2020a, 2020b).

In recent years, the use of boron-doped diamond (BDD) anodes in environmental protection areas have been widely investigated (Murugananthan *et al.* 2008; Pacheco *et al.* 2011; Rabaaoui *et al.* 2013; Fernandes *et al.* 2014; Antonin *et al.* 2015; Yang *et al.* 2016; Fudala-Ksiazek *et al.* 2018; Garcia-Espinoza *et al.* 2018). BDD anodes show high chemical stability in harsh environments including high voltage and current densities (Chen *et al.* 2003; Yang *et al.* 2016). During the electrolysis process, BDD anodes are able to produce weakly adsorbed hydroxyl radicals (•OH) from water oxidation. The producing •OH is the most oxidizing species after fluorine ($E° = 2.8$ V VERSUS the standard hydrogen electrode (SHE)), and it can unselectively mineralize many organic compounds (Pacheco *et al.* 2011), thereby showing advantages in mineralization efficiency compared with other anode materials, such as platinum (Pt), graphite felt, and dimensionally stable anodes (DSA) i.e., titanium and ruthenium oxide–iridium(IV) oxide (Ti/RuO_2-IrO_2)) (Sopaj *et al.* 2016). Several studies have used BDD anodes to degrade DCF. Brillas *et al.* (2010) reported that the use of BDD anodes with a lower current could significantly promote the total organic carbon (TOC) abatement of DCF compared with Pt anodes in a neutral buffer medium. Another study found

that a TOC removal of about 90% could be obtained for all studied DCF concentrations using BDD electrodes (Ihos *et al.* 2015). But these studies focused more on comparing BDD with other anodes on TOC removal without systematic research on the influencing factors and degradation pathways. Further study on the influencing factors, degradation products, degradation pathways, and degradation mechanism of DCF implemented by BDD anodes is still needed.

In this study, a series of comparative experiments was carried out to achieve three primary objectives: (1) to investigate the degradation characteristics of DCF in the electrochemical advanced oxidation process using BDD anodes; (2) to examine the effects of water quality parameters and operating parameters (i.e., humic acid (HA), bicarbonate (HCO_3^-), chloride ion (Cl^-), pH, electrolyte activity, current density, electrode spacing) on the electrochemical degradation; and (3) to identify the main degradation products and the DCF degradation pathway in electrochemical process using BDD anodes. The results contribute to understanding the mechanism and influencing factors of DCF degradation by niobium (Nb)/BDD anodes, and provide reference for the practical application of electrochemical treatment on pharmaceutical wastewater.

MATERIALS AND METHODS

Chemicals and materials

Diclofenac sodium ($C_{14}H_{10}Cl_2NNaO_2$) and HA were purchased from Sigma Aldrich (St. Louis, MO, USA). High-performance liquid chromatography (HPLC) grade methanol (MeOH) was supplied by Merck (Darmstadt, Germany). Sodium sulfate (Na_2SO_4), sodium chloride (NaCl), sodium bicarbonate ($NaHCO_3$), sodium nitrate ($NaNO_3$), disodium hydrogen phosphate (Na_2HPO_4), sodium dihydrogen phosphate (NaH_2PO_4) and tertiary butanol (TBA) were analytical grade and obtained from Sinopharm Chemical Reagent Co. Ltd (Shanghai, China). All solutions were prepared with ultrapure water, with a resistivity of at least 18.2 MΩ cm^{-1}, produced from a Millipore purification system (Billerica, CA, USA), and stored at 4 °C in the dark.

Electrochemical experiments

Electrolysis experiments were carried out in an undivided cylindrical cell made of polymethyl methacrylate. Two pieces of bipolar Nb/BDD electrode (10 cm × 5 cm × 2 mm, 6 μm coating thickness with 2,500 ppm boron doping) were purchased from NeoCoat company (La Chaux-de-Fonds, Switzerland). The effective electrode surface area submerged in the solution was 40 cm^2. Solutions containing 30 mmol L^{-1} Na_2SO_4 were used as the electrolyte. Constant current was supplied by an eTM-K8011SPL DC power (eTommens, China). A stir bar was placed inside the cell and a magnetic stirring apparatus (AS ONE, Japan) was used to ensure that the solution was well mixed.

The initial solution pH was adapted by 0.1 mol L^{-1} sodium hydroxide (NaOH) or sulfuric acid (H_2SO_4). The buffer solution was not used because it may interfere with the electrolysis process. Two electrodes were placed face to face with a gap of 2 cm. 50 μmol L^{-1} DCF and electrolyte were added to 1,000 mL of reaction solution. To compare the effects of different electrolytes, $NaNO_3$ and NaH_2PO_4 were selected and added to the same initial conductivity as 30 mmol L^{-1} Na_2SO_4. After the reaction solution was thoroughly mixed, experiments were initiated by applying a certain constant current. At predetermined time intervals, samples were withdrawn and filtered through a 0.22-μm polytetra fluoroethylene membrane before analysis. All experiments were performed at room temperature and conducted at least twice to ensure consistency.

Analytical methods

The pH, temperature, and conductivity values of the reaction solution were measured using a HQ40-d multi-parameter water analyzer (Hach, Loveland, CO, USA). DCF was analyzed using an Agilent 1260 HPLC (Agilent Technologies, Santa Clara, CA, USA) equipped with an Eclipse XDB-C18 analytical column (4.6 × 150 mm, 5 μm particle size) and a photodiode array detector. The mobile phase with a flow rate of 1 mL min^{-1} consisted of 30% formic acid hydroxide solution (0.1%, v/v) and 70% MeOH. The detection wavelength was 276 nm. Scanning electron microscopy (SEM) and Raman spectra analysis were performed using a Hitachi Regulus 8100 SEM (Hitachi, Ltd, Japan) and Thermo Fisher DXR2 Raman spectrometer (Thermo Fisher Scientific, USA).

The transformation products (TPs) were purified and concentrated by a solid phase extraction (SPE) workstation (Supelco Analytical, Bellefonte, PA, USA) with a 3 cc/60 mg Waters HLB cartridge (Waters, Corporation, Milford, MA, USA), and were identified through analysis using HPLC coupled with electrospray ionization (ESI) and quadrupole time-of-flight (qTOF) mass spectrometry (MS). Equipment used was the Ultimate 3000 HPLC (Thermo Fisher Scientific, Waltham, MA, USA), and the maXis Q-TOF-MS (Bruker AXS, Karlsruhe, Germany) with an ESI interface operated in the positive ion

mode (ESI+)). Detailed procedures of SPE, further information about the mobile phase operation condition, and operating parameters of HPLC-ESI-qTOF-MS were noted in Text S1, Table S1, and Text S2 in supplementary material.

RESULTS AND DISCUSSION

Transformation mechanism and degradation pathways

Roles of sulfate radicals and hydroxyl radicals

Early experiments show that there was no obvious loss of DCF for several hours in the 30 mmol L^{-1} of SO_4^{2-} solution without current. With the direct current power supplied, the decline of DCF followed the pseudo-first-order kinetics with an obvious kinetics constant of 0.0429 min^{-1} ($C_0 = 50$ μmol L^{-1}, Table 1). Two other types of electrolytes which could not be oxidized or reduced in this electrochemical process, nitrate (NO_3^-) and phosphate (PO_4^{3-}) which had the same conductivity, were compared with SO_4^{2-} (Figure S1). Results show that the kinetics constants dropped to 0.0263 min^{-1} (NO_3^-) and 0.0111 min^{-1} (PO_4^{3-}), which were 61.3% and 25.9% of the kinetics constants in the reaction using SO_4^{2-} as the electrolyte. After 30 min reaction, the removal rates of DCF were 73.0% (SO_4^{2-}), 52.7% (NO_3^-), and 28.6% (PO_4^{3-}), respectively (see Table 1).

The degradation of DCF with SO_4^{2-} was much faster than with PO_4^{3-} or NO_3^-. PO_4^{3-} may act as a scavenger of •OH and the resulting radicals or products which were unable to oxidize DCF. Chen *et al.* (2018) also found that the degradation of 2,4-dichlorophenol (2,4-DCP) was much faster in Na_2SO_4 than in the $NaNO_3$ medium. The presence of SO_4^{2-} led to the formation of the sulfate radical ($SO_4^{\bullet-}$) by direct electron transfer or oxidation by •OH produced during the electrochemical process. The presence of •OH and $SO_4^{\bullet-}$ in the electrolysis process with BDD anodes by electron spin-resonance spectroscopy experiments using 5,5-dimethyl-1-pyrroline-1-oxide as a trapping agent has been confirmed (Chen *et al.* 2018). $SO_4^{\bullet-}$ has a high standard oxidation–reduction potential (2.6 V versus normal hydrogen electrode) and a longer half-life (Avetta *et al.* 2015; Luo *et al.* 2019). Aniline-based pharmaceuticals (DCF and sulfamethoxazole) can quickly react with the $SO_4^{\bullet-}$ with second-order kinetic rate constants in the 9–10 × 10^9 M^{-1} s^{-1} range (Ahmed *et al.* 2012).

To further clarify the contributions of different radical species, quenching experiments were also carried out. MeOH and TBA are widely used to distinguish the contribution of •OH and $SO_4^{\bullet-}$. The kinetics constants that MeOH reacts with •OH and $SO_4^{\bullet-}$ were 9.7 × 10^8 $M^{-1}s^{-1}$ and 3.2 × 10^6 $M^{-1}s^{-1}$, respectively (Eibenberger *et al.* 1978; Buxton *et al.* 1988). For TBA, the kinetics constants were 3.8–7.6 × 10^8 $M^{-1}s^{-1}$ (•OH) and 4–9.1 × 10^5 $M^{-1}s^{-1}$($SO_4^{\bullet-}$) (Buxton *et al.* 1988; Neta *et al.* 1988). The constant of TBA reacting with •OH was almost three orders of a magnitude higher than that with $SO_4^{\bullet-}$. Therefore, MeOH served as an effective quencher for both •OH and $SO_4^{\bullet-}$, while TBA served as an effective quencher for •OH.

The addition of MeOH inhibited the degradation of DCF (Figure 1(a)), with the kinetic constants dropping to 0.0110 min^{-1} (1 mmol L^{-1}), 0.0106 min^{-1} (100 mmol L^{-1}), 0.0073 min^{-1} (500 mmol L^{-1}), and 0.0077 min^{-1} (1 mol L^{-1}) (Table S2). When the concentrations of MeOH were above 500 mmol L^{-1}, the kinetic constant was generally stable, indicating the quench of radicals to be sufficient. The addition of TBA also significantly inhibited the degradation of DCF (Figure 1(b)), with the kinetic constants dropping to around 0.0100 min^{-1} (1–500 mmol L^{-1}) (Table S2). 1 mmol L^{-1} of TBA can cause a sharp decline in the kinetic constant and removal rate. When the added TBA or MeOH was 500 mmol L^{-1}, the relative contributions of •OH, $SO_4^{\bullet-}$, and others (absorbed •OH, absorbed $SO_4^{\bullet-}$, direct electron transfer, etc) to the degradation of DCF are modeled with Equation (1). The kinetic constants were 0.0328 min^{-1} ($k_{\bullet OH}$), 0.0028 min^{-1} ($k_{SO_4^{\bullet-}}$), and 0.0073 min^{-1}(k_{others}), accounting for 76.5%, 6.5%, and 17.0% of the degradation kinetics of DCF (Figure 2), respectively. MeOH and TBA only quenched the radicals in bulk solution, but were unable to effectively scavenge the surface-adsorbed radicals (Solomon & Madix 1987; Barazesh *et al.* 2016; Wang *et al.* 2020). The radicals in the bulk solution caused about 83% of the DCF degradation

Table 1 | Kinetics of DCF degradation by Nb/BDD electrolysis employing different electrolytes

pH	Electrolytes	Concentration of electrolytes (mmol L^{-1})	Current density (mA cm^{-2})	Electrode distance (cm)	Kinetic constant (min^{-1})	Goodness of kinetic fit (R^2)	Removal rate (%)
7	NO_3^-	57	50	2	0.0263	0.9904	52.7
7	PO_4^{3-}	53.3	50	2	0.0111	0.9974	28.6
7	SO_4^{2-}	30	50	2	0.0429	0.9688	73.0

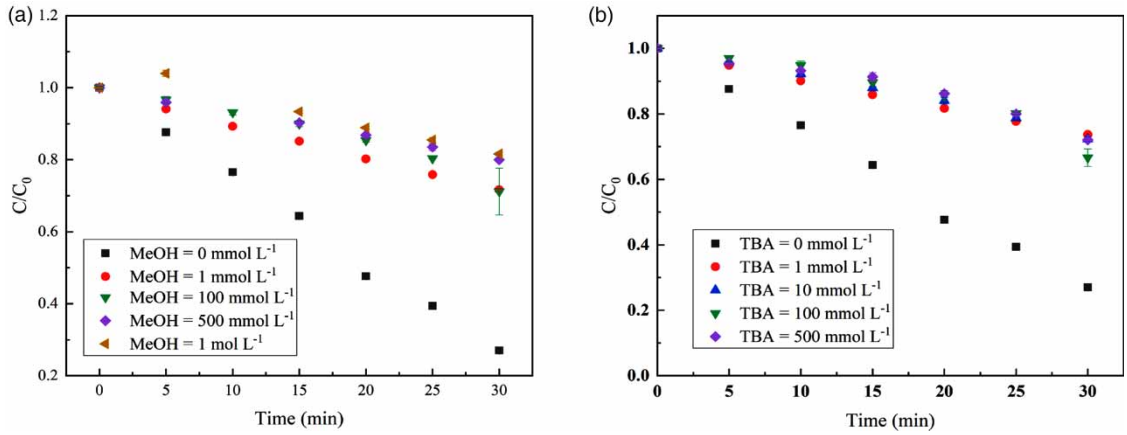

Figure 1 | Effects of MeOH and TBA on the degradation of DCF by Nb/BDD electrolysis. Concentration at time 0 is C_0(DCF) = 50 μmol L^{-1}, $C_0(Na_2SO_4)$ = 30 mmol L^{-1}, pH at time 0 is $pH_0 = 7$, current density j = 50 mA cm^{-2}, and electrode spacing l = 2 cm.

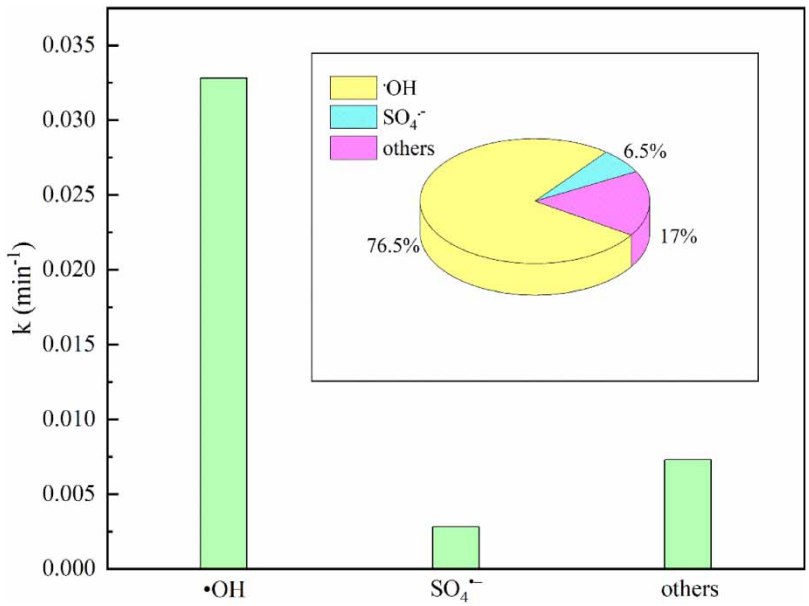

Figure 2 | Contributions of radicals in DCF electrolysis by Nb/BDD.

in this process. Absorbed radicals or direct electron transfer on the BDD anode surface also played important roles (17%).

$$k_{obs} = k_{\bullet OH} + k_{SO_4^{\bullet -}} + k_{others} \quad (1)$$

Degradation pathways of DCF

The total ion current chromatogram is shown in Figure S2 at different reaction times (0, 15, 30, and 40 min) of the SPE-concentrated sample from DCF degradation by BDD electrolysis process. Figure S2 (0 min) shows the retention time of DCF as 14.4 min. Figures S3 and S4 shows the mass spectrum and proposed structures of DCF and its main products detected by HPLC-ESI-qTOF-MS (ESI+). Eight TPs were identified, namely TP341, TP330, TP328, TP314, TP310 (two isomers), and TP266 (two isomers). The natural isotopic density of ^{35}Cl and ^{37}Cl satisfied the 3:1 ratio, which can help to identify the number of chlorine atoms in the TPs. The isotopic peak relative intensity of DCF (m/z 296), TP310, TP328, TP341, and

TP266 show a ratio 9:6:1, which verifies the presence of two chlorine atoms. Moreover, the isotopic peak relative density of ^{35}Cl and ^{37}Cl of TP330 and TP314 satisfied the ratio 27:27:9:1, demonstrating the presence of three chlorine atoms in these TPs. The production of TP328 was also detected in the oxidation of DCF by aqueous chlorine dioxide (Wang *et al.* 2014, 2015b). Given there is no extra chlorine atom addition in the electrolysis process, the emergence of TPs containing three chlorine atoms suggests dechlorination and chlorine oxidation processes in the BDD electrolysis. The m/z of TP341 was 45 Da more than DCF, possibly caused by the substituent of $-NO_2$ on the benzene ring, which was also detected in DCF abiotic and biotic processes in enriched nitrifying sludge (Wu *et al.* 2019). The substituent of $-NO_2$ may suggest the release of N from DCF cleavage because there was no extra N addition in this process. Two types of TP310 with different retention times suggests two different replacement positions of O on the benzene ring, which have also been detected in other research (Ahmed *et al.* 2012; Nie *et al.* 2014; Loos *et al.* 2018). The m/z of TP328 were 32 Da (2 −OH) more than DCF, and three different retention times indicate the presence of three isomers of different substituent modes of −OH on the benzene ring. The same phenomenon was also present in TP341, TP310, and TP266. According to the mass spectrum information and other reference research, the DCF degradation pathway in BDD electrolysis proposed is shown in Figure 3. According to the degradation products detected by liquid chromatography–mass spectrometry, hydroxylation, and decarboxylation are main pathways in DCF degradation, and dechlorination, chlorination, and nitro substitution were also part of this process.

Kinetics and influencing factors of DCF degradation by the Nb/BDD electrolysis process

Effects of initial pH on DCF degradation

The kinetic constants and removal rate of DCF degradation with different initial pH values are listed in Table 2. Figure 4(a) shows the effects of the initial pH on DCF degradation. DCF degradation was accelerated with the increase of initial pH values when pH values were between 6 and 10. The kinetics constants were 0.1087 min^{-1} (pH 10) > 0.0766 min^{-1} (pH 9) > 0.0507 min^{-1} (pH 8)> 0.0429 min^{-1} (pH 7) > 0.0384 min^{-1} (pH 6). When the initial pH was 5, the kinetics constant was 0.0964 min^{-1} (between the constants at pH 9 and pH 10). The removal of DCF after a 30 min reaction period reflected the same tendency as 99.8% (pH 10) > 93.6% (pH 5) > 90.2% (pH 9) > 77.7% (pH 8) > 73.0% (pH 7) > 68.3% (pH 6). DCF degradation was faster in an acidic or alkaline environment than in a neutral one, and the optimal pH for degradation was pH 10.

Chen *et al.* (2018) reported that $SO_4^{\bullet-}$ showed better oxidizing ability in alkaline conditions than in acidic conditions, and tended to be converted to •OH in alkaline conditions (Equations (2) and (3)). Li *et al.* (2020b) found that the

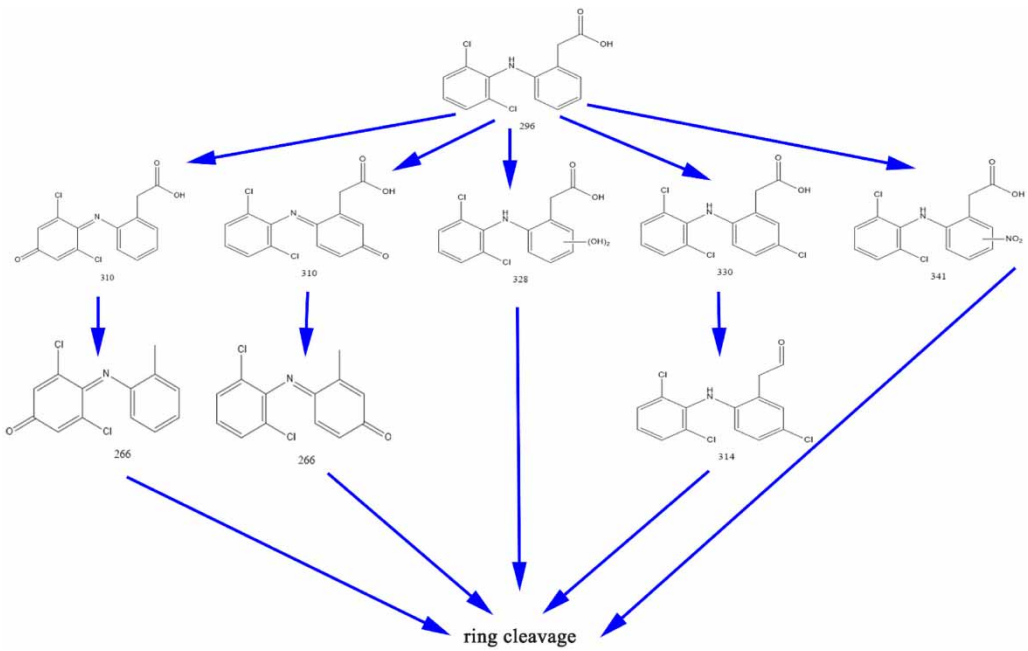

Figure 3 | Proposed degradation pathways of DCF.

Table 2 | Pseudo-first-order kinetics of DCF degradation by Nb/BDD electrolysis

pH	Electrolyte	Concentration of electrolyte (mmol L^{-1})	Current density (mA cm^{-2})	Electrode distance (cm)	Kinetic constant (min^{-1})	Goodness of kinetic fit (R^2)	Removal rate (%)
5	SO_4^{2-}	30	50	2	0.0964	0.9691	93.6
6	SO_4^{2-}	30	50	2	0.0384	0.9847	68.3
7	SO_4^{2-}	30	50	2	0.0429	0.9688	73.0
8	SO_4^{2-}	30	50	2	0.0507	0.9825	77.7
9	SO_4^{2-}	30	50	2	0.0766	0.9567	90.2
10	SO_4^{2-}	30	50	2	0.1087	0.9743	99.8
7	SO_4^{2-}	10	50	2	0.0166	0.9634	37.9
7	SO_4^{2-}	20	50	2	0.0306	0.9782	57.5
7	SO_4^{2-}	50	50	2	0.0635	0.9228	88.0
7	SO_4^{2-}	30	20	2	0.0090	0.9972	22.6
7	SO_4^{2-}	30	30	2	0.0108	0.9930	27.6
7	SO_4^{2-}	30	100	2	0.1965	0.9877	100
7	SO_4^{2-}	30	50	0.5	0.0339	0.9547	66.3
7	SO_4^{2-}	30	50	1	0.0678	0.9890	89.5

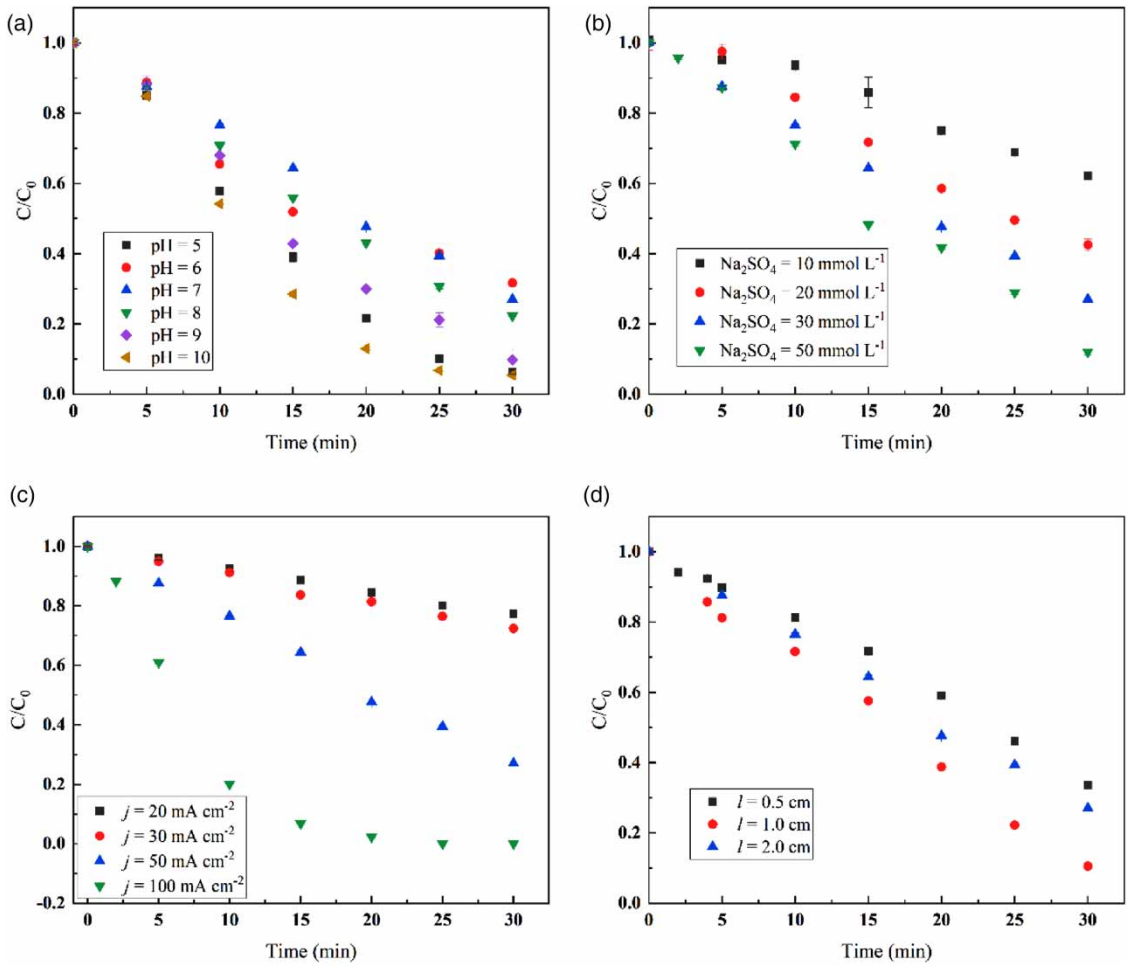

Figure 4 | Effects of initial pH (a), electrolyte concentration (b), current density (c), and electrode spacing (d) on the degradation of DCF by Nb/BDD electrolysis.

photodegradation of DCF followed a downward trend with the increase of pH in the range of 5.0–9.0, and explained that the absorption rate of DCF onto the surface of the photocatalyst would be higher in its molecular form than in its ionic form. The *p*Ka of DCF acid was 4.2 (Huber *et al.* 2003; Wang *et al.* 2015a). When pH <4.2, DCF_0 was the major form. When 4.2< pH <6.0, DCF^0 (molecular morphology) and DCF^- (negative valence) both served as dominating forms. When pH > 6.0, DCF^- became the vital species when present in water (Li *et al.* 2020b). In other research using carbon film-supported reduced graphene oxide-supported copper electrode anodes (Kumar *et al.* 2020), acidic conditions promoted the electro-oxidation of DCF. Considering the weakness of BDD anodes in absorption and the radicals in the bulk solution causing a DCF degradation of about 83% in this process, an increase in pH would promote both DCF^- dissolution and diffusion, enabling DCF^- to sufficiently react with the radicals in the bulk solution.

$$SO_4^{\bullet -} + H_2O \rightarrow SO_4^{2-} + \bullet OH + H^+ \quad k < 2.0 \times 10^8\ M^{-1}\ s^{-1} \tag{2}$$

$$SO_4^{\bullet -} + OH^- \rightarrow SO_4^{2-} + \bullet OH \quad k = 6.5 \times 10^7\ M^{-1}\ s^{-1} \tag{3}$$

Effects of electrolyte concentration on DCF degradation

The effect of electrolyte concentration on DCF degradation is shown in Figure 4(b). The degradation of DCF accelerates with the increase of electrolyte concentration (10 mmol L^{-1} to 50 mmol L^{-1}). Table 2 lists the kinetics constants as 0.0633 min^{-1} (50 mmol L^{-1}) > 0.0429 min^{-1} (30 mmol L^{-1}) > 0.0306 min^{-1} (20 mmol L^{-1}) > 0.0166 min^{-1} (10 mmol L^{-1}). The removal of DCF after a 30 min reaction reflects the same tendency as 88.0% (50 mmol L^{-1}) > 73.0% (30 mmol L^{-1}) > 57.5% (20 mmol L^{-1}) > 37.9% (10 mmol L^{-1}). The increase of electrolyte concentration increases the conductivity, as well as promotes the production of $SO_4^{\bullet -}$, which accelerates the electrodegradation of DCF. Chen *et al.* (2018) also found that along with the SO_4^{2-} concentration increasing from 0.01 to 0.2 M, the apparent rate constants of 2,4-DCP electrolysis increased from 0.48 to 1.38 h^{-1}.

Effects of current density on DCF degradation

The effect of current density on DCF degradation is shown in Figure 4(c). The increase of current density promotes the degradation of DCF (20 mA cm^{-2} to 100 mA cm^{-2}). The kinetic constants are 0.1965 min^{-1} (100 mA cm^{-2}) > 0.0429 min^{-1} (50 mA cm^{-2}) > 0.0108 min^{-1} (30 mA cm^{-2}) > 0.0090 min^{-1} (20 mA cm^{-2}) (Table 2). After a 30 min reaction, the DCF degradation reached 73.0% (50 mA cm^{-2}), 27.6% (30 mA cm^{-2}), and 22.6% (20 mA cm^{-2}) and was completely removed when the current density was 100 mA cm^{-2}.

The increase of current density could improve the generation of radicals via electron transfer. This phenomenon has also been found in electrochemical degradation processes of losartan (Salazar *et al.* 2016), sulfamethazine (Barhoumi *et al.* 2016; Sopaj *et al.* 2016), ifosfamide (Fabiańska *et al.* 2015), and nitrobenzene (Rabaaoui *et al.* 2013). The increase of current density resulted in a higher concentration of •OH in the bulk solution (Komtchou *et al.* 2017). In addition, the BDD anode can extend the range of current densities and significantly raise the most optimal current density compared to Pt and DSA anodes due to its very high O_2 evolution over potential and weak adsorption of BDD(•OH) (Sopaj *et al.* 2016). A significant temperature increase (24.6 °C) was observed after 30 min of electrolysis when the current density was set at 100 mA cm^{-2}, which was more than for other temperature changes (+2.3 °C (20 mA cm^{-2}), +2.9 °C (30 mA cm^{-2}), and +9.1 °C (50 mA cm–2)). Some researchers also found that the higher temperature significantly enhances the removal rate of contaminants, including DCF, by accelerating the diffusion and transfer of radicals, contaminants, and byproducts in electrolysis (Coledam *et al.* 2016; Liu *et al.* 2018; Loos *et al.* 2018) and the ClO_2 oxidation process (Wang *et al.* 2015b). In this paper, the increase of temperature at high current density may further promote the degradation of DCF.

Effects of electrode spacing on DCF degradation

Figure 4(d) and Table 2 show the effects of electrode spacing on DCF degradation. Notably, degradation kinetic constants were 0.0339 min^{-1} (0.5 cm), 0.0678 min^{-1} (1 cm), and 0.0429 min^{-1} (2 cm), and the removal rates of DCF after 30 min reaction were 66.3% (0.5 cm), 89.5% (1 cm), and 73.0% (2 cm). The best spacing was 1 cm, which suggests that spacing electrodes too close together may inhibit the diffusion of free radicals and DCF in the bulk solution, and influence the following reaction.

Effects of typical dissolved substances on DCF degradation

HCO_3^-, Cl^-, and HA are typical dissolved substances in water which may interface with the free radical oxidation process. Figure 5(a) shows the effect of HCO_3^- on DCF degradation. The addition of HCO_3^- significantly inhibits its degradation as the kinetic constants are reduced from 0.0507 min^{-1} to 0.0312 min^{-1}(0.1 mmol L^{-1}) and 0.161 min^{-1} (1 mmol L^{-1}) (Table 3). The removal rates reduced from 77.7% to 59.6% (0.1 mmol L^{-1}) and 38.9% (1 mmol L^{-1}). The addition of HCO_3^- resulted in the consumption of •OH to produce $•CO_3^-$, which acts as a selective oxidation species, but with a much lower reaction rate constant than that of $SO_4^{•-}$ and •OH for the oxidation process of organic pollutants (Orellana-García *et al.* 2015; Barazesh *et al.* 2016; Xiao *et al.* 2016; Fu *et al.* 2019). The reaction rate constants of $•CO_3^-$ (a one-electron oxidant, $E_0 =$ 1.78 V at pH 7) with several typical organic compounds are in the range of 10^6–10^7 $M^{-1}s^{-1}$ (e.g. atrazine, fluometuron, tertbutryn, and diurona) and thus, on average, slower compared to 10^8–10^{10} $M^{-1}s^{-1}$ for $SO_4^{•-}$ and/or •OH (Arciprete *et al.* 2012; Luo *et al.* 2019). HCO_3^- therefore mainly scavenges $SO_4^{•-}$ and •OH, resulting in a decreased oxidation rate of organic compounds (Fabiańska *et al.* 2015), as well as DCF. Li *et al.* (2020c) also found that HCO_3^- showed an inhibitory effect on electrocatalytic hydrodechlorination of DCF using polypyrrole-reduced graphene oxide (PPy-rGO) modified Pd-Ni bimetallic electrodes. When 5 mmol L^{-1} of HCO_3^- were added, the kinetic constant and removal rate were lower than with 0.1 mmol L^{-1} of HCO_3^- added but higher than with 1 mmol L^{-1} of HCO_3^-. This addition of 5 mmol L^{-1} HCO_3^- also increased conductivity, which could promote the electrolysis process. The weakened inhibition of 5 mmol L^{-1} HCO_3^- may therefore be a combination of these two different effects.

The addition of HA significantly inhibited the removal of DCF (Figure 5(b), Table 3). The kinetic constants were 0.0330 min^{-1}(0.1 mg L^{-1}), 0.0187 min^{-1} (1 mg L^{-1}), and 0.0170 min^{-1} (5 mg L^{-1}). The DCF removal rates reduced to 61.7% (0.1 mg L^{-1}), 42.2% (1 mg L^{-1}), and 38.0% (5 mg L^{-1}). Generally, natural organic matter (NOM) reacts with free radicals

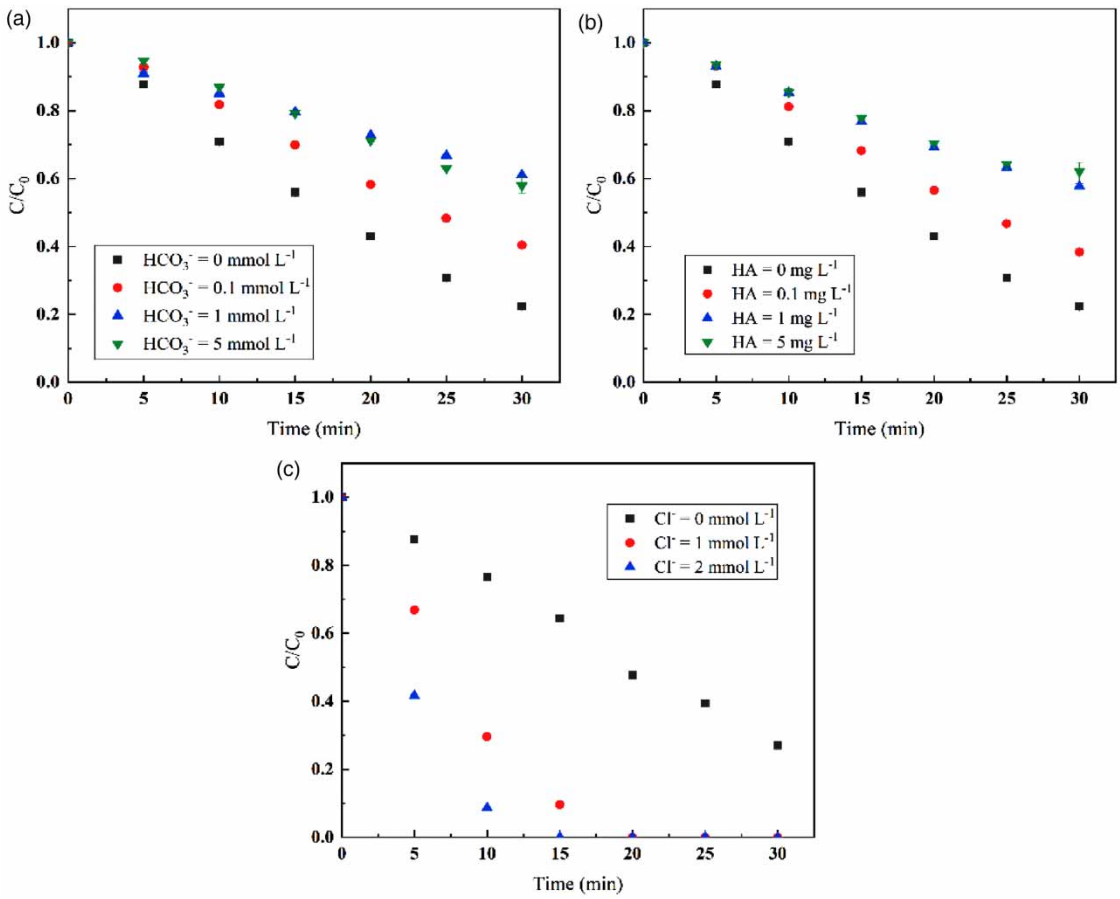

Figure 5 | Effects of typical dissolved substances (a: HCO_3^-; b: HA; c: Cl^-) on the degradation of DCF by Nb/BDD electrolysis. C_0(DCF) = 50 μmol L^{-1}, $C_0(Na_2SO_4) = 30$ mmol L^{-1}, $pH_0 = 7$ or 8, $j = 50$ mA cm^{-2}, and $l = 2$ cm.

Table 3 | Influence of typical dissolved substances on kinetics of the DCF degradation by Nb/BDD electrolysis

pH	Typical dissolved substance	Concentration	Kinetic constant (min^{-1})	Goodness of kinetic fit (R^2)	Removal rate (%)
7	–	–	0.0429	0.9688	73.0
7	Cl^-	1 mmol L^{-1}	0.1566	0.9593	100
7	Cl^-	2 mmol L^{-1}	0.2446	0.9738	100
8	–	–	0.0507	0.9825	77.7
8	HCO_3^-	0.1 mmol L^{-1}	0.0312	0.9850	59.6
8	HCO_3^-	1 mmol L^{-1}	0.0161	0.9973	38.9
8	HCO_3^-	5 mmol L^{-1}	0.0190	0.9908	42.1
8	HA	0.1 mg L^{-1}	0.0330	0.9849	61.7
8	HA	1 mg L^{-1}	0.0187	0.9978	42.2
8	HA	5 mg L^{-1}	0.0170	0.9910	38.0

and inhibits the degradation of contaminants (Barazesh *et al.* 2016; Xiao *et al.* 2016; Ji *et al.* 2018; Li *et al.* 2020b). Ahn *et al.* (2017) experimentally determined the rate constants of Suwanner River NOM with $SO_4^{\bullet-}$ ($k_{SO4}^{\bullet-}/NOM = 4.50 \times 10^6$ $M^{-1}s^{-1}$) and •OH ($k_{\bullet OH}/NOM = 3.30 \times 10^8$ $M^{-1}s^{-1}$). NOM affects the oxidation reaction based on radicals through scavenging radicals and reversing the radicals intermediates to the parent compound (Lutze *et al.* 2015; Feng *et al.* 2017). Komtchou *et al.* (2017) also found that HA competed with the contaminant and its by-products during water treatment. Thus, the inhibited degradation of DCF was expected in this study.

The addition of Cl^- significantly promoted the removal of DCF (Figure 5(c), Table 3). The addition of 1 mmol L^{-1} Cl^- yielded a 100% removal within 20 min of electrolysis reaction. With 2 mmol L^{-1} of Cl^- added, it was 15 min. The kinetics constants reached 0.1566 min^{-1}(1 mmol L^{-1}) and 0.2446 min^{-1}(2 mmol L^{-1}), which is almost 3.6 and 5.7 times more than the reaction without Cl^- added, respectively. The concentrations of Cl^- also show good linear correlation ($r^2 = 0.995$) with kinetics constants (Figure 6). Ridruejo *et al.* (2018) also reported that Cl^- accelerated the decay of tetracaine in the electrochemical Fenton process with the RuO_2-based anode. Cl^- reacts with •OH to generate •Cl (Equations (4) and (5), and the Cl adsorbate shows significantly lower adsorption energy (−4.161 and −3.851 eV) than the OH adsorbate (−7.891 and −8.801 eV), suggesting that •Cl is more easily released than •OH on BDD (001) and the desorbed •Cl could participate in contaminant degradation (Wang *et al.* 2020). As a result, the presence of Cl^- accelerated the degradation of DCF. Other research reported that the addition of 10 mmol L^{-1} Cl^- enhanced the loss rates of trace organic contaminants (atrazine, carbamazepine, sulfamethoxazole, acesulfame, etc.) due to rapid reactions with electrochemically generated HClO from Cl^-, as

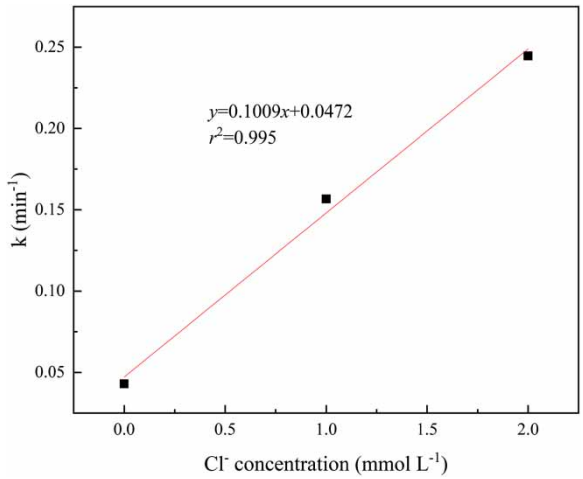

Figure 6 | Linear fit analysis of the addition of Cl^- and kinetic constants.

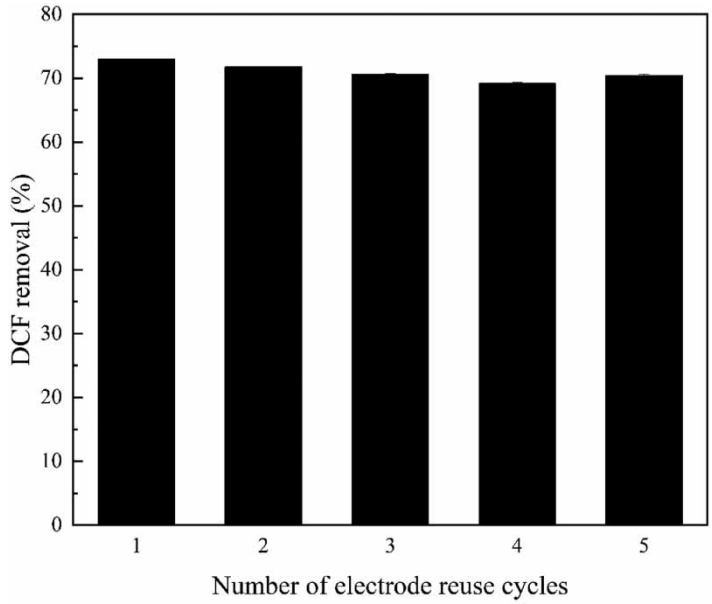

Figure 7 | DCF removal by Nb/BDD electrode for five consecutive cycles. C_0(DCF) = 50 μmol L^{-1}, C_0(Na_2SO_4) = 30 mmol L^{-1}, $pH_0 = 7$, j = 50 mA cm^{-2}, and l = 2 cm.

expressed in Equations (6) and (7) (Barazesh *et al.* 2016; Jalife-Jacobo *et al.* 2016). Among the TPs of DCF, products containing three Cl atoms were identified, suggesting the participation of oxidizing substances containing Cl^- in this electrochemical process. Cl^- plays an important promoting role in this process, indicating that the electrochemical degradation by BDD anodes could be a good choice for trace contaminant removal in waters with high concentration of Cl^-. Given that the ocean is an important and final sink of NSAIDs, experiments carried out in real seawater showed a rapid removal of 50 μmol L^{-1} DCF, reaching a 100% removal rate within 5 min with the same operating parameters (Figure S5).

$$\bullet OH + Cl^- \rightarrow \bullet ClHO^- \quad (4)$$

$$\bullet ClHO^- + H^+ \rightarrow \bullet Cl + H_2O \quad (5)$$

$$2Cl^- \rightarrow Cl_2 + 2e^- \quad (6)$$

$$Cl_2 + H_2O \rightarrow HClO + Cl^- + H^+ \quad (7)$$

Reusability study

The reusability of the Nb/BDD electrode was also studied. The reusability capacity of the Nb/BDD electrode for DCF degradation was investigated for five consecutive cycles (Figure 7). The degradation capacity remained stable, showing a slightly decrease of DCF removal from 73% to 69% after five cycles. SEM and Raman analyses before and after degradation cycles were carried out and are shown in Figure S6. The BDD film remained dense without obvious damage after five cycles (Figure S6(b)) compared to the film before reaction (Figure S6(a)). Raman spectra after five cycles indicated that the small amount of graphite on the surface was oxidized or removed during the anodizing process, with the absence of the peak at 1,580 cm^{-1}, while the signal for diamond was still strong (Figure S6(c) and (d)), demonstrating good stability of BDD.

CONCLUSIONS

The degradation of DCF by BDD anodes have proven a good fit for the pseudo-first-order degradation kinetics. Both acidic and alkaline conditions promoted the DCF degradation. The degradation was also promoted by the increase of electrolyte concentration and current density. HA and HCO_3^- significantly inhibited the degradation of DCF, whereas Cl^- accelerated the degradation of DCF. •OH, $SO_4^{\bullet-}$, and others contributed 76.5%, 6.5%, and 17.0% of the degradation kinetics of DCF,

respectively. •OH contributed more than $SO_4^{\bullet-}$ in this process. Major TPs of DCF were identified. According to the degradation products detected by liquid chromatography–mass spectrometry, hydroxylation, dechlorination, and decarboxylation are the main pathways to DCF degradation, and chlorination and nitro substitution are also included in degradation process.

ACKNOWLEDGEMENTS

This work was supported by the Shandong Provincial Natural Science Foundation (No. ZR2017BB037, 2018ZRLD007) and the National Natural Science Foundation of China (No. 31300414 and No. U2006209).

DATA AVAILABILITY STATEMENT

All relevant data are included in the paper or its Supplementary Information.

REFERENCES

Ahmed, M., Barbati, S., Doumenq, P. & Chiron, S. 2012 Sulfate radical anion oxidation of DCF and sulfamethoxazole for water decontamination. *Chem. Eng. J.* **197**, 440–447.

Ahn, Y., Lee, D., Kwon, M., Choi, I. H., Nam, S. N. & Kang, J. W. 2017 Characteristics and fate of natural organic matter during UV oxidation processes. *Chemosphere* **184**, 960–968.

Ali, I., AL-Othmanb, Z. A. & Alwarthan, A. 2016 Synthesis of composite iron nano adsorbent and removal of ibuprofen drug residue from water. *J. Mol. Liq.* **219**, 858–864.

Antonin, V. S., Santos, M. C., Garcia-Segura, S. & Brillas, E. 2015 Electrochemical incineration of the antibiotic ciprofloxacin in sulfate medium and synthetic urine matrix. *Water Res.* **83**, 31–41.

Arciprete, M. L. D., Soler, J. M., Santos-Juanes, L., Arques, A., Mártire, D. O., Furlong, J. P. & Gonzalez, M. C. 2012 Reactivity of neonicotinoid insecticides with carbonate radicals. *Water Res.* **46**, 3479–3489.

Aslan, M., Kirimlioglu, E., Afşar, E., Çeker, T. & Yılmaz, C. 2020 Increased PUFA levels in kidney epithelial cells in the course of DCF toxicity. *Toxicol. in Vitro.* https://doi.org/10.1016/j.tiv.2020.104836.

Avetta, P., Pensato, A., Minella, M., Malandrino, M., Maurino, V., Minero, C., Hanna, K. & Vione, D. 2015 Activation of persulfate by irradiated magnetite: implications for the degradation of phenol under heterogeneous photo-Fenton-like conditions. *Environ. Sci. Technol.* **49** (2), 1043–1050.

Balasubramani, K., Sivarajasekar, N. & Naushad, M. 2020 Effective adsorption of antidiabetic pharmaceutical (metformin) from aqueous medium using graphene oxide nanoparticles: equilibrium and statistical modelling. *J. Mol. Liq.* **301**, 112426.

Barazesh, J. M., Prasse, C. & Sedlak, D. L. 2016 Electrochemical transformation of trace organic contaminants in the presence of halide and carbonate ions. *Environ. Sci. Technol.* **50** (18), 10143–10152.

Barhoumi, N., Oturan, N., Olvera-Vargas, H., Brillas, E., Gadri, A., Ammar, S. & Oturan, M. A. 2016 Pyrite as a sustainable catalyst in electro-Fenton process for improving oxidation of sulfamethazine. Kinetics, mechanism and toxicity assessment. *Water Res.* **94**, 52–61.

Brillas, E., Garcia-Segura, S., Skoumal, M. & Arias, C. 2010 Electrochemical incineration of DCF in neutral aqueous medium by anodic oxidation using Pt and boron-doped diamond anodes. *Chemosphere* **79**, 605–612.

Buxton, G. V., Greenstock, C. L., Helman, W. P. & Ross, A. B. 1988 Critical review of rate constants for reactions of hydrated electrons, hydrogen atoms and hydroxyl radicals (•OH/•O^-) in aqueous solution. *J. Phys. Chem. Ref. Data* **17**, 513–886.

Chen, X., Chen, G., Gao, F. & Yue, P. L. 2003 High-performance Ti/BDD electrodes for pollutant oxidation. *Environ. Sci. Technol.* **37**, 5021–5026.

Chen, L., Lei, C., Li, Z., Yang, B., Zhang, X. & Lei, L. 2018 Electrochemical activation of sulfate by BDD anode in basic medium for efficient removal of organic pollutants. *Chemosphere* **210**, 516–523.

Coledam, D. A. C., Aquino, J. M., Silva, B. F., Silva, A. J. & Rocha-Filho, R. C. 2016 Electrochemical mineralization of norfloxacin using distinct boron-doped diamond anodes in a filter-press reactor, with investigations of toxicity and oxidation by-products. *Electrochim. Acta.* **213**, 856–864.

Dhiman, P., Kumar, A., Shekh, M., Sharma, G., Rana, G., Vo, D.-V. N., AlMasoud, N., Naushad, M. & ALOthman, Z. A. 2021 Robust magnetic ZnO-Fe_2O_3 Z-scheme hetereojunctions with in-built metal-redox for high performance photo-degradation of sulfamethoxazole and electrochemical dopamine detection. *Environ. Res.* **197**, 111074.

Duarte, I. A., Reis-Santos, P., Novais, S. C., Rato, L. D., Lemos, M. F. L., Freitas, A., Pouca, A. S. V., Barbosa, J., Cabral, H. N. & Fonseca, V. F. 2020 Depressed, hypertense and sore: long-term effects of fluoxetine, propranolol and DCF exposure in a top predator fish. *Sci. Total Environ.* https://doi.org/10.1016/j.scitotenv.2020.136564.

Eibenberger, H., Steenken, S., O'Neill, P. & Schulte-Frohlinde, D. 1978 Pulse radiolysis and electron spin resonance studies concerning the reaction of $SO_4^{\bullet-}$ with alcohols and ethers in aqueous solution. *J. Phys. Chem.* **82**, 749–750.

Fabiańska, A., Ofiarska, A., Fiszka-Borzyszkowska, A., Stepnowski, P. & Siedlecka, E. M. 2015 Electrodegradation of ifosfamide and cyclophosphamide at BDD electrode: decomposition pathway and its kinetics. *Chem. Eng. J.* **276**, 274–282.

Feng, Y., Song, Q., Lv, W. & Liu, G. 2017 Degradation of ketoprofen by sulfate radical-based advanced oxidation processes: kinetics, mechanisms, and effects of natural water matrices. *Chemosphere* **189**, 643–651.

Fent, K., Weston, A. & Caminada, D. 2006 Ecotoxicology of human pharmaceuticals. *Aquat. Toxicol.* **76** (2), 122–159.

Fernandes, A., Santos, D., Pacheco, M. J., Ciríaco, L. & Lopes, A. 2014 Nitrogen and organic load removal from sanitary landfill leachates by anodic oxidation at Ti/Pt/PbO_2, Ti/Pt/SnO_2-Sb_2O_4 and Si/BDD. *Appl. Catal. B: Environ.* **148–149**, 288–294.

Fu, Y. Y., Wu, G., Geng, J. J., Li, J. C., Li, S. N. & Ren, H. Q. 2019 Kinetics and modeling of artificial sweeteners degradation in wastewater by the UV/persulfate process. *Water Res.* **150**, 12–20.

Fu, Q., Fedrizzi, D., Kosfeld, V., Schlechtriem, C., Ganz, V., Derrer, S., Rentsch, D. & Hollender, J. 2020 Biotransformation changes bioaccumulation and toxicity of DCF in aquatic organisms. *Environ. Sci. Technol.* **54** (7), 4400–4408.

Fudala-Ksiazek, S., Sobaszek, M., Luczkiewicz, A., Pieczynska, A., Ofiarsk, A., Fiszka-Borzyszkowska, A., Sawczak, M., Ficek, M., Bogdanowicz, R. & Siedlecka, E. M. 2018 Influence of the boron doping level on the electrochemical oxidation of raw landfill leachates. *Chem. Eng. J.* **334**, 1074–1084.

Garcia-Espinoza, J. D., Mijaylova-Nacheva, P. & Aviles-Flores, M. 2018 Electrochemical carbamazepine degradation: effect of the generated active chlorine, transformation pathways and toxicity. *Chemosphere* **192**, 142–151.

Huber, M. M., Canonica, S., Park, G. & Gunten, U. V. 2003 Oxidation of pharmaceuticals during ozonation and advanced oxidation processes. *Environ. Sci. Technol.* **37**, 1016–1024.

Ihos, M., Manea, F., Jitaru, M., Bogatu, C. & Pode, R. 2015 Diclofenac removal from aqueous solutions by electrooxidation ar boron-doped diamond (BDD) electrode. *Environ. Eng. Manag. J.* **14** (6), 1339–1345.

Jalife-Jacobo, H., Feria-Reyes, R., Serrano-Torres, O., Gutierrez-Granados, S. & Peralta-Hernandez, J. M. 2016 Diazo dye Congo Red degradation using a Boron-doped diamond anode: an experimental study on the effect of supporting electrolytes. *J. Hazard. Mater.* **319**, 78–83.

Ji, Y., Yang, Y., Zhou, L., Wang, L., Lu, J., Ferronato, C. & Chovelon, J. M. 2018 Photodegradation of sulfasalazine and its human metabolites in water by UV and UV/peroxydisulfate processes. *Water Res.* **133**, 299–309.

Komtchou, S., Dirany, A., Drogui, P., Robert, D. & Lafrance, P. 2017 Removal of atrazine and its by-products from water using electrochemical advanced oxidation processes. *Water Res.* **125**, 91–103.

Kreuzinger, N., Clara, M., Strenn, B. & Kroiss, H. 2004 Relevance of the sludge retention time (SRT) as design criteria for wastewater treatment plants for the removal of endocrine disruptors and pharmaceuticals from wastewater. *Water Sci. Technol.* **50** (5), 149–156.

Kumar, A., Omar, R. A. & Verma, N. 2020 Efficient electro-oxidation of DCF persistent organic pollutant in wastewater using carbon film-supported Cu-rGO electrode. *Chemosphere.* https://doi.org/10.1016/j.chemosphere.2020.126030.

Li, J., Wang, H., Qi, Z., Ma, C., Zhang, Z., Zhao, B., Wang, L., Zhang, H., Chong, Y., Chen, X., Cheng, X. & Dionysiou, D. D. 2020a Kinetics and mechanisms of electrocatalytic hydrodechlorination of DCF on Pd-Ni/PPy-rGO/Ni electrodes. *Appl. Catal. B: Environ.* https://doi.org/10.1016/j.apcatb.2020.118696.

Li, S., Wang, Z., Xie, X., Liang, G., Cai, X., Zhang, X. & Wang, Z. 2020b Fabrication of vessel-like biochar-based heterojunction photocatalyst Bi_2S_3/BiOBr/BC for DCF removal under visible LED light irradiation: mechanistic investigation and intermediates analysis. *J. Hazard. Mater.* https://doi.org/10.1016/j.jhazmat.2019.121407.

Li, J., Wang, H., Qi, Z., Ma, C., Zhang, Z., Zhao, B., Wang, L., Zhang, H., Chong, Y., Chen, X., Cheng, X. & Dionysiou, D. D. 2020c Kinetics and mechanisms of electrocatalytic hydrodechlorination of DCF on Pd-Ni/PPy-rGO/Ni electrodes. *Appl. Catal. B: Environ.* **268**, 118696.

Lindqvist, N., Tuhkanen, T. & Kronberg, L. 2005 Occurrence of acidic pharmaceuticals in raw and treated sewages and in receiving waters. *Water Res.* **39** (11), 2219–2228.

Lishman, L., Smyth, S. A., Sarafin, K., Kleywegt, S., Toito, J., Peart, T., Lee, B., Servos, M., Beland, M. & Seto, P. 2006 Occurrence and reductions of pharmaceuticals and personal care products and estrogens by municipal wastewater treatment plants in Ontario, Canada. *Sci. Total Environ.* **367** (2–3), 544–558.

Liu, Z., Zhao, C., Wang, P., Zheng, H., Sun, Y. & Dionysiou, D. D. 2018 Removal of carbamazepine in water by electro-activated carbon fiber-peroxydisulfate: comparison, optimization, recycle, and mechanism study. *Chem. Eng. J.* **343**, 28–36.

Loos, G., Scheers, T., Van Eyck, K., Van Schepdael, A., Adams, E., Van der Bruggen, B., Cabooter, D. & Dewil, R. 2018 Electrochemical oxidation of key pharmaceuticals using a boron doped diamond electrode. *Sep. Purif. Technol.* **195**, 184–191.

Luo, C., Gao, J., Wu, D., Jiang, J., Liu, Y., Zhou, W. & Ma, J. 2019 Oxidation of 2,4-bromophenol by UV/PDS and formation of bromate and brominated products: a comparison to UV/H_2O_2. *Chem. Eng. J.* **358**, 1342–1350.

Lutze, H. V., Bircher, S., Rapp, I., Kerlin, N., Bakkour, R., Geisler, M., von Sonntag, C. & Schmidt, T. C. 2015 Degradation of chlorotriazine pesticides by sulfate radicals and the influence of organic matter. *Environ. Sci. Technol.* **49** (3), 1673–1680.

Murugananthan, M., Yoshihara, S., Rakuma, T. & Shirakashi, T. 2008 Mineralization of bisphenol A (BPA) by anodic oxidation with boron-doped diamond (BDD) electrode. *J. Hazard. Mater.* **154** (1–3), 213–220.

Neta, P., Huie, R. E. & Ross, A. B. 1988 Rate constants for reactions of inorganic radicals in aqueous solution. *J. Phys. Chem. Ref. Data* **17** (3), 1027–1284.

Nie, E., Yang, M., Wang, D., Yang, X., Luo, X. & Zheng, Z. 2014 Degradation of DCF by ultrasonic irradiation: kinetic studies and degradation pathways. *Chemosphere* **113**, 165–170.

Oaks, J. L., Gilbert, M., Virani, M. Z., Watson, R. T., Meteyer, C. U., Rideout, B. A., Shivaprasad, H. L., Ahmed, S., Chaudhry, M. J. I., Arshad, M., Mahmood, S., Ali, A. & Khan, A. A. 2004 Diclofenac residues as the cause of vulture population decline in Pakistan. *Nature* **427**, 4.

Orellana-García, F., Alvarez, M. A., Lopez-Ramon, M. V., Rivera-Utrilla, J. & Sanchez-Polo, M. 2015 Effect of $HO^{\bullet}$, $SO_4^{\bullet-}$ and $CO_3^{\bullet-}/HCO_3^{\bullet}$ radicals on the photodegradation of the herbicide amitrole by UV radiation in aqueous solution. *Chem. Eng. J.* **267**, 182–190.

Owumi, S. E., Aliyu-Banjo, N. O. & Odunola, O. A. 2020 Selenium attenuates DCF-induced testicular and epididymal toxicity in rats. *Andrologia*. https://doi.org/10.1111/and.13669.

Pacheco, M. J., Santos, V., Ciríaco, L. & Lopes, A. 2011 Electrochemical degradation of aromatic amines on BDD electrodes. *J. Hazard. Mater.* **186** (2–3), 1033–1041.

Rabaaoui, N., Moussaoui, Y., Allagui, M. S., Ahmed, B. & Elaloui, E. 2013 Anodic oxidation of nitrobenzene on BDD electrode: variable effects and mechanisms of degradation. *Sep. Purif. Technol.* **107**, 318–323.

Ridruejo, C., Centellas, F., Cabot, P. L., Sires, I. & Brillas, E. 2018 Electrochemical Fenton-based treatment of tetracaine in synthetic and urban wastewater using active and non-active anodes. *Water Res.* **128**, 71–81.

Salazar, C., Contreras, N., Mansilla, H. D., Yanez, J. & Salazar, R. 2016 Electrochemical degradation of the antihypertensive losartan in aqueous medium by electro-oxidation with boron-doped diamond electrode. *J. Hazard. Mater.* **319**, 84–92.

Sharma, G., Gupta, V. K., Agarwal, S., Bhogal, S., Naushad, M., Kumar, A. & Stadler, F. J. 2018 Fabrication and characterization of trimetallic nano-photocatalyst for remediation of ampicillin antibiotic. *J. Mol. Liq.* **260**, 342–350.

Solomon, J. L. & Madix, R. J. 1987 Kinetics and mechanism of the oxidation of allyl alcohol on Ag(110). *J. Phys. Chem.* **91** (24), 6241–6244.

Sopaj, F., Oturan, N., Pinson, J., Podvorica, F. & Oturan, M. A. 2016 Effect of the anode materials on the efficiency of the electro-Fenton process for the mineralization of the antibiotic sulfamethazine. *Appl. Catal. B: Environ.* **199**, 331–341.

Stuer-Lauridsen, F., Birkved, M., Hansen, L. P., Lutzhoft, H. C. H. & Halling-Sorensen, B. 2000 Environmental risk assessment of human pharmaceuticals in Denmark after normal therapeutic use. *Chemosphere* **40** (7), 783–793.

Tauxe-Wuersch, A., De Alencastro, L. F., Grandjean, D. & Tarradellas, J. 2005 Occurrence of several acidic drugs in sewage treatment plants in Switzerland and risk assessment. *Water Res.* **39** (9), 1761–1772.

Wang, Y. L., Liu, H. J., Liu, G. G. & Xie, Y. H. 2014 Oxidation of DCF by aqueous chlorine dioxide: identification of major disinfection byproducts and toxicity evaluation. *Sci. Total Environ.* **473**, 437–445.

Wang, Y., Liu, H., Liu, G., Xie, Y. & Ni, T. 2015a Oxidation of DCF with chlorine dioxide in aquatic environments: influences of different nitrogenous species. *Environ. Sci. Pollut. Res. Int.* **22** (12), 9449–9456.

Wang, Y., Liu, H., Xie, Y., Ni, T. & Liu, G. 2015b Oxidative removal of DCF by chlorine dioxide: reaction kinetics and mechanism. *Chem. Eng. J.* **279**, 409–415.

Wang, L., Lu, J., Li, L., Wang, Y. & Huang, Q. 2020 Effects of chloride on electrochemical degradation of perfluorooctanesulfonate by Magneli phase Ti_4O_7 and boron doped diamond anodes. *Water Res.* https://doi.org/10.1016/j.watres.2019.115254.

Wu, G., Geng, J., Li, S., Li, J., Fu, Y., Xu, K., Ren, H. & Zhang, X. 2019 Abiotic and biotic processes of DCF in enriched nitrifying sludge: kinetics, transformation products and reactions. *Sci. Total Environ.* **683**, 80–88.

Xiao, Y., Zhang, L., Zhang, W., Lim, K. Y., Webster, R. D. & Lim, T. T. 2016 Comparative evaluation of iodoacids removal by UV/persulfate and UV/H_2O_2 processes. *Water Res.* **102**, 629–639.

Yang, N., Foord, J. S. & Jiang, X. 2016 Diamond electrochemistry at the nanoscale: a review. *Carbon* **99**, 90–110.

Zhang, Y., Geißen, S.-U. & Gal, C. 2008 Carbamazepine and DCF: removal in wastewater treatment plants and occurrence in water bodies. *Chemosphere* **73** (8), 1151–1161.

Zorita, S., Martensson, L. & Mathiasson, L. 2009 Occurrence and removal of pharmaceuticals in a municipal sewage treatment system in the south of Sweden. *Sci. Total Environ.* **407** (8), 2760–2770.

First received 31 March 2021; accepted in revised form 5 June 2021. Available online 17 June 2021